JOURNAL OF ELECTROCARDIOLOGY

Supplement on Magnetocardiography

Part II
Magnetic Field Produced by a Current Dipole

By David Cohen, Ph.D.* and Hidehiro Hosaka, M.S.†

SUMMARY

To understand the MCG, electrical models of the heart must be used in which the basic building-block is usually the current dipole. The dipole's magnetic field is generally made up of two parts: 1. the contribution by the dipole element itself, which is mathematically simple; 2. the contribution by the current generated in the volume conductor by the dipole, which is complicated and depends on the boundaries; for special boundaries this contribution is zero to Bz, the component of magnetic field which is normal to the boundary. This applies to the boundaries of the semi-infinite volume conductor, the infinite slab, and the sphere. This property allows great simplification in solving the magnetic forward and inverse problems. Because of its importance, it is proven with electrolytic tank experiments. Based on this property, a method is presented for estimating the presence of those dipole combinations which produce a suppressed surface potential; it consists of a visual examination of an "arrow" display of Bz.

Now that the magnetcardiogram (MCG) has been mapped from a variety of subjects,[1,2] the next step is to extract new information from these maps.[3,4] A preliminary approach to this problem has been to compare visually the MCG maps with the ECGs of these subjects.[2] However, for more utility, explicit heart generators which produced the magnetic field must ultimately be found; these are the solutions to the magnetic inverse problem. As a first step toward finding these solutions, we have been studying the basic element used in models which simulate the current sources in the heart; this element is the current dipole.

We have been studying the magnetic field produced by the current dipole located in volume conductors of several elementary shapes. These are the most basic magnetic forward

*Senior Scientist, Francis Bitter National Magnet Laboratory, Massachusetts Institute of Technology, Cambridge, Massachusetts.
†Senior Project Engineer, Nihon Kohden Kogyo Company, Ltd., Tokyo, Japan.

problems, and they prepare us for the inverse problems. Most of this paper deals with one property of the magnetic field around these shapes. Although models with current dipoles have already been used in solving some types of forward[5,6] and inverse magnetic problems,[6,7] the investigators using these models were not aware of the property described here; their results and interpretation could have been simplified. We believe that future work with the inverse problem will take this property into account.

The current dipole is illustrated in Fig. 1. The dipole generates ion current, called the volume current, in the surrounding volume conductor. The total magnetic field of the dipole is produced both by this volume current and by the current element of the dipole itself. We express this as

$$\vec{B}=\vec{B}_v+\vec{B}_d \qquad (1)$$

where $\vec{B}$ is the magnetic vector at any field point, and the subscripts v and d denote the separate contributions from the volume current and dipole element. However, with special shapes of volume conductor, we will demonstrate that the contribution of $\vec{B}_v$ to one or more components of the external field $\vec{B}$ is zero; these components of $\vec{B}$ are therefore due only to the dipole current element. This is an unusual and important property, allowing great simplification in the solutions of both the forward and inverse problems for these shapes. Although some investigators had been aware of this property, its significance may not have been realized, and it had not been previously published. We also show some applications of this property to the forward and inverse problem of the heart's magnetic field.

In paper III of this group we change from these special shapes of volume conductor to the shape of the human torso; it is shown that this special property is still approximately maintained, with some restrictions. In paper IV we use this property to find, in a simple way, solutions to the inverse magnetic problem from the MCG maps of two normal and one abnormal subject.

THEORY OF THE CURRENT DIPOLE

The current dipole is a directed line element $\vec{\Delta l}$ which generates a current in the surrounding volume conductor. By definition $\Delta l << r$ where Δl is the dipole length and r is the distance from the dipole to any measuring point P. The current i passes through the dipole into the volume conductor; the quantity $i\vec{\Delta l}$ is finite and is called the dipole moment. The current dipole is distinct from a magnetic dipole, which is a small current loop (see Addendum to Part IV). In an infinite homogeneous volume conductor, the current dipole generates a current density

$$\vec{J}=-\vec{\nabla}\left(\frac{i\vec{\Delta l}\cdot\hat{r}}{4\pi r^2}\right)=\frac{i\Delta l}{4\pi r^3}\left(\hat{r}2\cos\theta+\hat{\theta}\sin\theta\right) \qquad (2)$$

where $\hat{r}$ and $\hat{\theta}$ are unit vectors in the radial and elevation directions; MKS units are used in this section.

We now describe the dipole's magnetic field when it is located in the simplest configuration of volume conductor, the infinite homogeneous conductor. There are various methods for deriving this field. Baule, in his thesis,[8] briefly considered the current dipole and used a standard method, which we also use here. To the section of spherical cap shown in Fig. 1 we apply Ampère's circuital law:

$$\oint \vec{B}\cdot\vec{dp}=\mu_o\int_S \vec{J}\cdot\vec{ds} \qquad (3)$$

where $\vec{B}$ is the field at the perimeter of the cap, $\vec{p}$ is the distance along the perimeter, $\vec{ds}$ is an element of cap surface area, and μ_o is

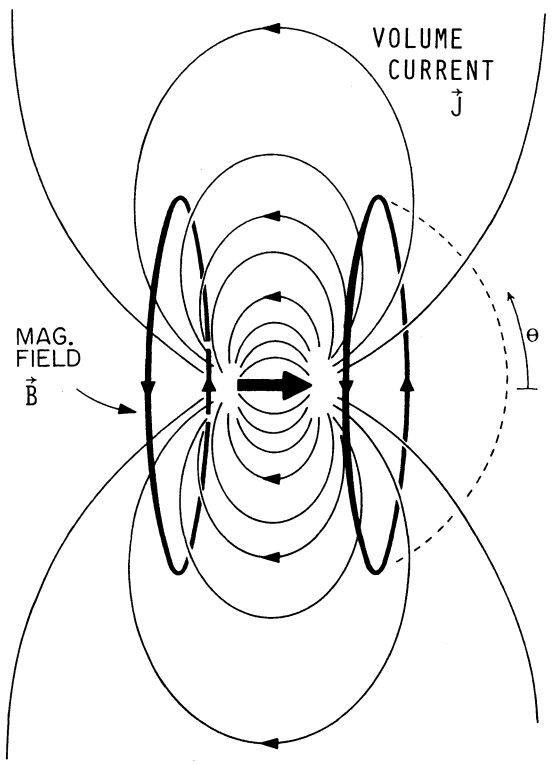

Fig. 1. Current dipole $i\vec{\Delta l}$ (heavy arrow) in an infinite volume conductor. It generates a volume current of density J. The magnetic field B (heavy circles) receives a net contribution of zero from the volume current, and is therefore due only to the dipole element $i\vec{\Delta l}$. The section of hemispherical cap (broken line) is used in eqn. (3).

the permeability of free space; the medium permeability is assumed to be unity. By putting $\vec{J}$ from (2) into (3), we get for the component of $\vec{B}$ along the perimeter:

$$B = \frac{\mu_o i \Delta l \sin\theta_o}{4\pi r^2} \qquad (4)$$

where θ_o is the angle to the perimeter. The other two components of $\vec{B}$ are zero due to current symmetry. This is identical to the differential form of the Biot-Savart Law which gives the element of field produced by an element of current $i\Delta l$. By comparison, therefore, the field at any point in the volume conductor is due only to the dipole element; $\vec{B}=\vec{B}_d$, hence $\vec{B}_v=0$. Unfortunately Baule did not comment on the value of this result and it was not published, in contrast to other portions of the thesis.[9]

Another method of showing this property, which is instructive and readily extended to other shapes, is due to D. W. Kerst.[10] The volume current of the dipole in an infinite homogeneous volume conductor can be considered to be the linear superposition of current from each pole separately; this is illustrated in Fig. 2. Using this, we evaluate the magnetic field at point P. Mathematically this field is the sum of three parts: the contribution from the current of the right-hand pole, of the left-hand pole, and from the dipole element $i\Delta l$. For the right-hand contribution we define three orthogonal components of field: B_r is in a direction radial to that pole, both B_r and B_θ are parallel to the page, while B_z is perpendicular. We then note that $B_r=B_\theta=B_z=0$ because of current symmetry, hence the right-hand contribution is zero. Similarly, with components for the left-hand pole, the left-hand contribution is zero. It follows that the total magnetic field is due only to $i\vec{\Delta l}$, as we wished to show. This proof does not depend on the condition $\Delta l << r$, but only on the existence of both a source and sink; hence it also applies to a bipole (poles far apart) and is more general than the previous derivation.

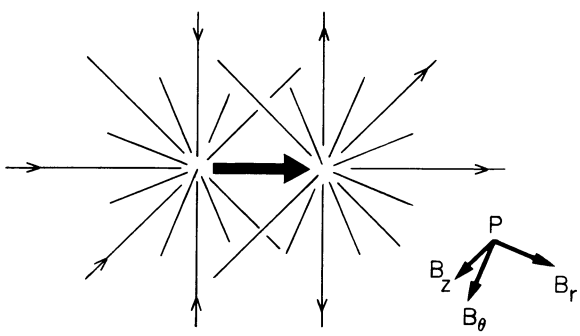

Fig. 2. An instructive way of considering the current dipole in an infinite volume conductor. The volume current, for example as in Fig. 1, is a linear superposition of straight-line current due to source and sink separately; these are shown as light, radiating lines.

We now extend this method to the case of a semi-infinite volume conductor. Let the boundary coincide with the page, and let the bipole be below and parallel to the page. We move the point P to a new location above the paper by a pure translation upward; $b\theta$ and B_z are therefore unchanged, but B_r changes to the projected $B_{r'}$ which is parallel to the page. We note again that $B_{r'}=B_z=0$ because of symmetry of current from the source, but now $B\theta\neq 0$. Because the same is true for components due to the sink current, only $B_z=0$ from both source and sink. The total B_z is therefore due only to the current within the bipole. This result holds if a second, parallel boundary is added, that is, for the shape of an infinite slab. This shape begins to approach the shape of the human torso. Some other special shapes or symmetrical conditions may be similarly shown to produce this property by using this method.

In yet another method, due to Geselowitz,[11] the contribution to $\vec{B}$ from only the volume current in any homogeneous conductor is given by the surface integral

$$\vec{B}_v = \frac{\mu_o \sigma}{4\pi} \int_S \frac{V\hat{r}}{r^2} \times \vec{ds} \qquad (5)$$

where V is the potential at the surface source point, $\vec{r}$ is the vector from this point to the external field point, and $\vec{ds}$ is an element of surface. We can directly apply this integral to the semi-infinite conductor and also to a conductor of spherical shape. For both cases, we see that the perpendicular component $B_{zv}=0$ because $\hat{r}\times\vec{ds}$ is tangential to the surface.

The property $B_{zv}=0$ can be visualized if we begin with an imaginary plane in an infinite volume conductor and a dipole parallel to and below this plane. Considering the dipole's magnetic field above the plane, we replace this plane by an actual boundary, with an insulator (say air) above the boundary. Due to this boundary a new magnetic field appears; it is always parallel to the boundary, at any distance above the boundary. The original normal component $B_z=B_{zd}$ is unchanged. If we add yet another boundary parallel to the first but below the dipole, yet another new, parallel field would appear.

The fact that $B_{zv}=0$ for the above configurations means that only eqn. (4) is involved in the solution of both the forward and inverse magnetic problem, if only the z-component of field is used. The complexity of

relating the field to the volume current is eliminated. In fact, the expression for B_z due to one or more underlying dipoles is now more simple than the expressions for the surface potential; the effect of the accumulated surface charges is *always* present in the potential. Also in the next paper it is shown, for the shape of the human torso, that although the volume-current contribution to the normal field component is not zero, it is somewhat less than the contribution of the surface charge to the potential. However, this small advantage is not enough to justify the use of the MCG. A much stronger justification is based on the fact that the distribution of B_z from a dipole is always at 90° to the distribution of the surface potential (which is identical, as shown in Fig. 7). As a result, those combinations of dipoles which produce suppressed surface potentials (compared with one dipole) may be detected magnetically more readily. This is because B_z will not be diminished for these combinations and may even be enhanced, due to the 90° rotation. Because of ever-present noise, these dipoles may be hidden from potential measurements, but readily revealed by B_z measurements, if B_{zv} can be ignored. The basic combination of this type, discussed later, is shown in the second row of Fig. 7.

EXPERIMENTAL VERIFICATION

Because of the importance of $B_{zv}=0$, experiments were performed in order to verify this property for a dipole in a semi-infinite medium. Verification of $B_{zv}=0$ for this case could be considered to be verification for the other shapes which, in theory, possess this property. The semi-infinite arrangement was simulated by a "large" electrolytic tank. The basic idea was to have a choice of two different generators: a current dipole complete with volume current, or only the volume current where the dipole element $i\Delta l$ was absent. These are shown in Fig. 3 as electrodes fed by wire pair a or b, respectively. When using pair a, the dipole element was the current in the section of wire between the two electrodes, hence both dipole element and return current were present. When using only wire pair b, the current in the vertical wires gave $B_z=0$ and the horizontal section at the bottom produced negligible field at the surface. B_z was therefore due only to the volume current, and this B_{zv} could be directly measured.

A number of different experiments were performed, four of which are described here. Either B_z or the quantity $\partial B_z/\partial y$ was measured. The reason for this latter measurement can be understood if we examine, in Fig. 6,

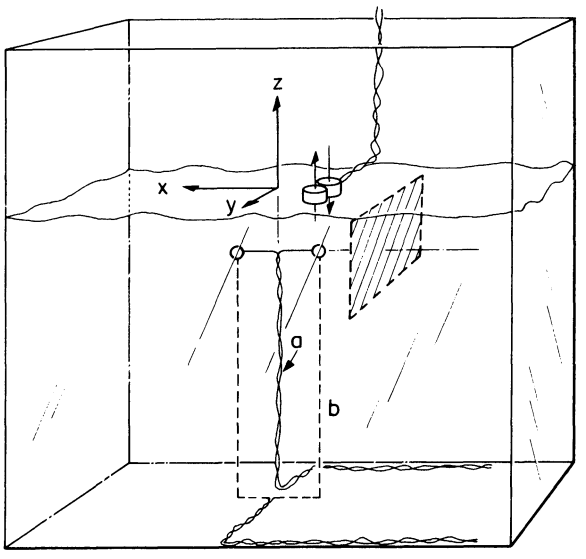

Fig. 3. Electrolytic tank used to verify $B_{zv}=0$. The two electrodes, shown with exaggerated separation, were fed ac by either pair of insulated wires, a or b. The quantities B_z or $\partial B_z/\partial y$ were measured by the voltage induced in either one coil, or both in series-opposition. A complete current dipole was simulated when pair a was used; pair b gave only the volume current. The shaded rectangle is an insulated sheet used to simulate a flat boundary.

the solid curves of B, C, and D, due to a single dipole. We note that $B_z=0$ just over the dipole. We then ask: What quantity is a maximum just over the dipole? We see that B_y is a maximum, but we cannot use this because it is "contaminated" by volume current. The next quantity is $\partial B_z/\partial y$, and this does fulfill our requirements. In some experiments this gradient is the best quantity to measure, not B_z. For example, in verifying eqn. (4) by measuring the decrease of B_z with z-distance from the dipole, the direct measure of B_z would necessitate a complicated y-placement of the detector. However, the measurement of falloff of $\partial B_z/\partial y$ with increasing z need simply be made on the vertical line $x=y=0$. The concept of $\partial B_z/\partial y$ and its maximum just over the dipole is the basis of the arrow map, used later.

The tank used for most of the measurements was plastic, roughly cubical, and about 1.5 meters on a side. The conductor was a simple NaCl solution with resistivity of about 30 ohm-cm. The electrodes were solder spheres separated by a distance which could be varied from 0.5 to 1.5 cm, and were fed by formvar-coated, stiff magnet wire. The current was 20 ma and alternating, with a frequency of 3kHz, generated by an audio amplifier fed by an oscillator. This system was very linear and gave a large signal relative to detector noise. Two identical coils were used as detectors, by means of the voltage induced by the alternating B_z. To measure B_z

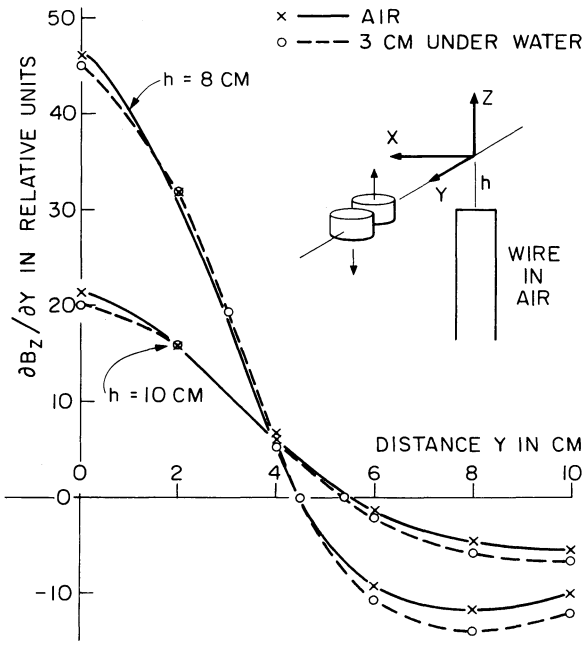

Fig. 4. Measurement of $\partial B_z/\partial y$ due to a horizontal current element in air, and due to the a-pair in the tank. The same current i and dipole length Δl were used in both. The gradiometer received a contribution only from the horizontal element; the two vertical wires each produced $B_z=0$ everywhere.

only one coil was used; both coils in series constituted a gradiometer which measured $\partial B_z/\partial y$. Each coil contained about 500 turns of thin magnet wire and was 2.5 cm in diameter and 1.6 cm in length. One or both coils fed a PAR tuned amplifier operating at Q=100. The rectified output signal was proportional to B_z or to $\partial B_z/\partial y$.

The first experiment consisted of a comparison between $\partial B_z/\partial y$ from the a-pair in the tank and from an equivalent dipole element completely in air, without volume current; the air arrangement is shown in Fig. 4. The purpose of this experiment was twofold. First, to calibrate and assess any problems in both the current system and detection system, using only a known $i\Delta l$ in air, without volume current. Second, as one method of detecting any significant contribution from the volume current in the tank; if $B_{zv}=0$ then the air and tank measurements would yield identical values of $\partial B_z/\partial y$, at any value of y. During the experiment care was taken with the wire shape in air to insure that the vertical members were straight, hence gave no contribution to B_z. To accomplish this, the vertical wires were run through long ceramic pipes of very small bore which then encased the wires and allowed fine adjustment of position and angle. The results are shown in Fig. 4. The gradiometer curves are seen to be identical in air and in conducting solution, to within experimental error. The curve shape is similar to the calculated $\partial B_z/\partial y$ curve in Fig. 6C, due to $i\Delta l$ only. The difference between the 8-cm and 10-cm spacing agrees with the z^{-3} falloff. The data, therefore, is in good agreement with $B_{zv}=0$.

The second measurement was again the falloff of $\partial B_z/\partial y$ with increasing z-distance, but for many points on the line x=y=0. Only the a-pair was used here. If $B_{zv}=0$ then eqn. (4) is valid and yields, by differentiation, a falloff which is z^{-3}. A perfect z^{-3} falloff does not uniquely prove that $B_{zv}=0$, but is strong supporting evidence. The result of this experiment was that $\partial B_z/\partial y$ does vary as z^{-3}, to within experimental error. The experimental data (not shown here) were clear.

The third experiment was performed in order to find the effect on B_z of a flat side boundary. The boundary was simulated by an insulating sheet of plastic, about 4 cm by 10 cm in area; it was first arranged in the y-z plane as illustrated in Fig. 3, then later in the x-z plane. The results would give preliminary information about the effect of the high-resistivity lung near the equivalent dipoles of the heart, which would yield a B_{zv} contribution. This B_{zv} relative to B_{zd} was determined as follows. First, B_{zd} (assumed) was measured with no insulator, by one coil at x=0, y=2.0 cm, using the a-pair; this was the approximate location of maximum B_z for the z-distance used here (see Fig. 6B). Then the a-pair was changed to the b-pair, with all spacing identical, yielding only B_{zv} (assumed). The experimental arrangement was considered satisfactory when $B_{zv}/B_{zd}\lesssim 0.02$. Now the insulator was used, and B_z was measured as a function of the x-spacing between the insulator and the electrodes. This sequence was repeated with the insulator moved by 90°, so that it was now in the x-z plane, and the y-position was varied.

The results of this third experiment were two curves, not shown here. The ordinate for both is the ratio B_{zv}/B_{zd}. As the x-position of the insulator is decreased, the first curve rises to $B_{zv}/B_{zd}=0.32$ at x=1.0 cm. As the y-position of the insulator is decreased, the second curve rises to a ratio of 0.42 at y=1.0 cm. These ratios show that the insulator strongly breaks the radial current symmetry, and that the high resistivity of the lung is capable of producing large B_{zv}.

In the fourth experiment, which was the most direct, B_z was measured from pair a and pair b, without and with a cylindrical boundary. The purpose was twofold: to measure directly B_{zv} relative to $B_{zd}+B_{zv}$ for the semi-infinite case, and to gain more information about a nearby boundary. The cylindrical

boundary is midway in approximation between the previous flat boundary and the actual lung, and was an open vertical plastic tube with a radius of 4 cm and length of about 8 cm. The top was just above the liquid surface; the electrodes were centered on the axis. A smaller tank was used than previously. A single coil measured B_z at a fixed x and z, but as a function of y. Without cylinder, the b-wires yielded a pure B_{zv} while the a-wires yielded pure B_{zd}. The phase of the detected signal with respect to phase of the oscillator was noted; this gave the relative polarity of B_z. Curves of B_z vs. y were obtained for these four arrangements: a-wires without cylinder (yielding $B_{zd}+B_{zv}$); b-wires without cylinder (yielding only B_{zv}); a-wires with cylinder (yielding $B_{zd}+B_{zv}$ with cylinder); b-wires with cylinder (yielding B_{zv} due to the cylinder).

The four measured curves are shown in Fig. 5. The uppermost curve ($B_{zd}+B_{zv}$) has the same shape as the solid curve of Fig. 6B, as it should if $B_{zv}=0$. The curve from the b-wires without cylinder, due only to B_{zv}, is seen to be about 5% of the upper curve, for $y \lesssim 5$ cm. This is the most direct evidence that B_{zv} is small relative to B_{zd}. For $y>5$ cm the effect of the smaller tank used here becomes apparent, and the approximation to a semi-infinite conductor breaks down. The lowest curve shows that the cylindrical insulator has a strong effect. The negative polarity confirms that the curve is due to volume current, which flows oppositely to the dipole element. The curve due to the a-wires with cylinder is seen to be the difference between the most upper and lower curves for $y \lesssim 5$ cm, as it should. This curve should simulate the variation of MCG amplitude across the chest, when the heart is approximated by a single dipole and the lung by a pure cylindrical insulator. However, it is seen to be similar to the uppermost curve (dipole element); this suggests that the actual MCG distribution across the chest may not be a strong function of the volume current. This distribution is computed in the next paper, using the simulated, inhomogeneous torso.

These experiments strongly confirm that $B_{zv}=0$ for the semi-infinite volume conductor. The dipole theory presented here is therefore confirmed. We may conclude that $B_{zv}=0$ for the other shapes mentioned, such as the infinite slab and the sphere.

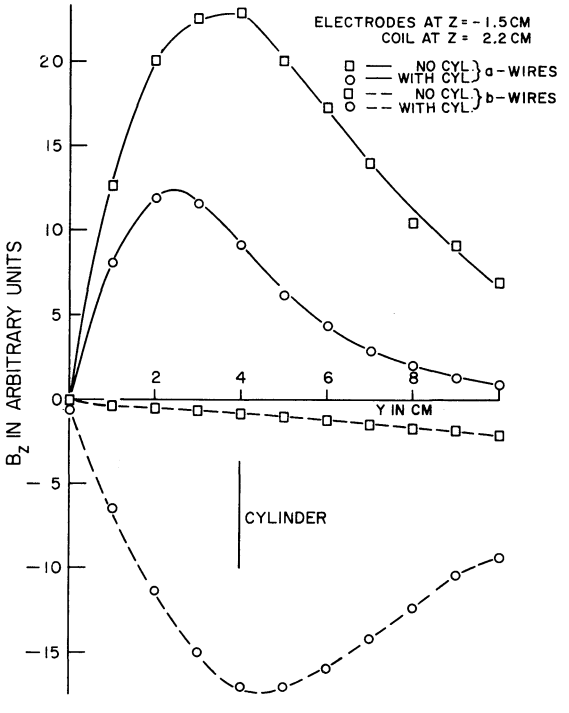

Fig. 5. Measurements of B_z at x=0, with and without insulating cylindrical boundary. Electrodes were centered on the cylinder axis, which was vertical. The present arrangement can be visualized as the insulator of Fig. 3 continued around the electrodes in a wrap-around fashion.

APPLICATIONS TO THE MCG

The property $B_{zv}=0$ can be used to explain some of the features of the human MCG. Because it is shown in the next paper that this property approximately holds for the human torso, it follows that $B_z \approx B_{zd}$ and that eqn. (4) is valid. One MCG feature which can be explained, for example, is the falloff of MCG amplitude with distance from the chest. The measured rate of falloff[12] is somewhat slower than z^{-2} over the heart region, with z=0 in the heart. Now it is known from potential mapping that the normal heart can be crudely approximated by a single dipole, at a time near the peak of QRS. Eqn. (4) can therefore be used to set up the expression for B_z, for this one dipole. We have done this and have found that the variation of B_z with z is in approximate agreement with the measured falloff. One can further use this information to relate the amplitude of the normal MCG to the thickness of the subject's chest. One would therefore have an MCG index which would be the counterpart of the ECG ponderal index, although different.

There is an important application of $B_{zv}=0$ when the heart is more accurately represented by a multi-dipole model. This property, because it simplifies solution to the magnetic inverse problem, can be used to determine (from MCG data) those dipole combinations which produce suppressed surface potentials.

A major justification for using the MCG is to find these combinations, suppressed on the ECG; we will therefore dwell on this application.

The basic dipole combination for this purpose is an opposing pair, as shown by the two (broken) dipoles in Fig. 6A. The computed Bz due to a single dipole and this pair is shown in Fig. 6B, where the ratio of maximum Bz is seen to be 0.5. Other calculations show that 0.14 is the same ratio of potential. A factor of about 3.5 is therefore the magnetic gain over the potential gain; this is independent of the dipole separation, for small separation. Although a gain of 3.5 is not particularly impressive, the gain increases greatly[4] as the number of dipoles is increased to three or more "around-a-loop." These, then are the combinations of two or more dipoles which are of interest to us.

We can ask: What are the best ways to detect the presence of these combinations from MCG measurements? In answer, we first point out that the MCG measurements should only be of the normal component and its derivatives (Bz, $\partial Bz/\partial y$, $\partial^2 Bz/\partial z^2$, etc.) so that the volume-current contribution will be small or negligible. This means that the boundary effects will be small or negligible (see Part III), hence torso changes from subject-to-subject can be ignored. We then note two approaches for detecting these combinations: 1. to obtain solutions of the inverse magnetic problem by methods of calculation; 2. less accurately, by methods involving visual estimation. With methods of calculation (matrix inversion, etc.) there is some advantage in using $\partial^2 Bz/\partial z^2$ data instead of Bz data. This can be seen in Fig. 6B, C, and D. While the ratios of Bz and $\partial Bz/\partial y$ from the pair/dipole are both about 0.5, this ratio for $\partial^2 Bz/\partial z^2$ is about unity. The second derivative is therefore enriched with dipole-pair information, which is an aid in terms of signal/noise of the calculations. A detector (gradiometer) which measures $\partial^2 Bz/\partial z^2$, while not yet a common instrument, has the added advantage of being insensitive to magnetic background and can therefore be used in hospitals and clinics. Some MCGs of this type have already been recorded.[12,13]

We next discuss methods of visual display and estimation. Say we have MCGs which have been recorded across the chest, using Bz, the field component normal to the chest (Bn is more general and is used in the subsequent papers). Because it is impractical to record MCGs with a grid spacing finer than about 5 cm, the well-known isopotential type of instantaneous map cannot be used here. Instead we have been using a map consisting of squares,[2,12] shown in the left and middle columns of Fig. 7. We here suggest an alternate

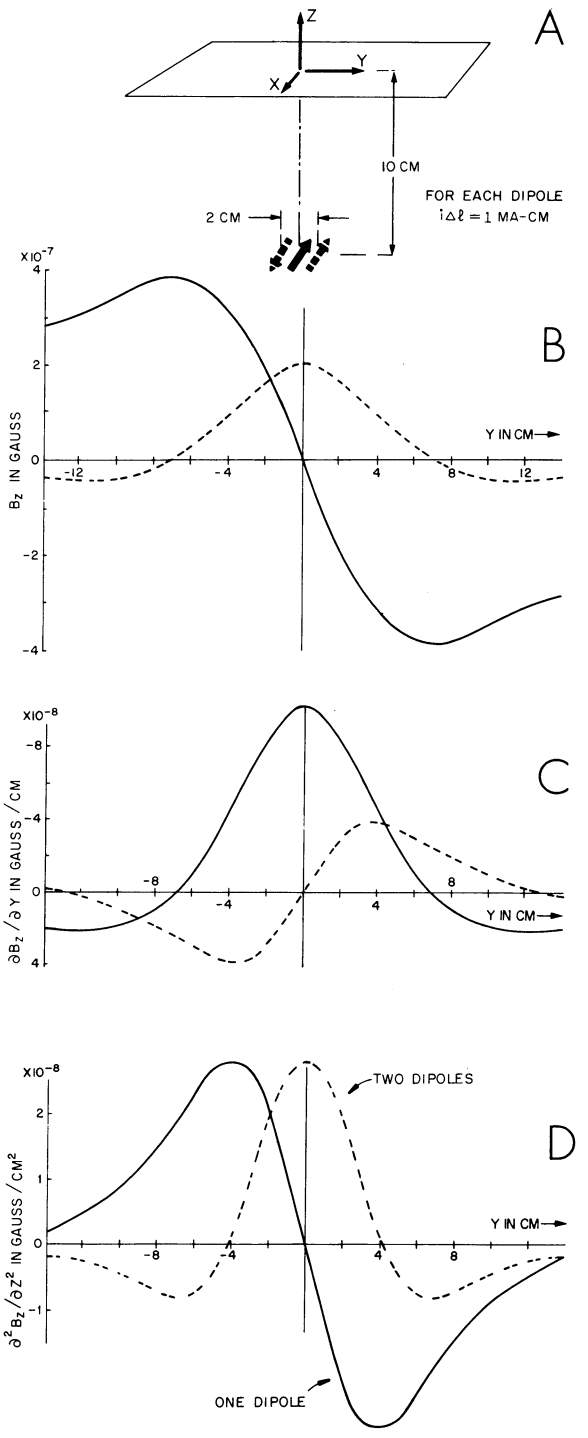

Fig. 6. Curves of Bz and its derivatives as a function of y, due to a single dipole (solid lines) and to an opposing dipole pair (broken lines). The quantity which has its maximum over a single dipole is $\partial Bz/\partial y$, which is therefore useful for measurements and for visual display of data. The quantity which is enriched in the ratio of two/one dipole is $\partial^2 Bz/\partial z^2$. The curves were computed from eqn. (4) and dimensions in A. For convenience, units are in guass and cm instead of MKS. Bz, its derivatives, and the electrical potential increase linearly with the distance between the dipole pair.

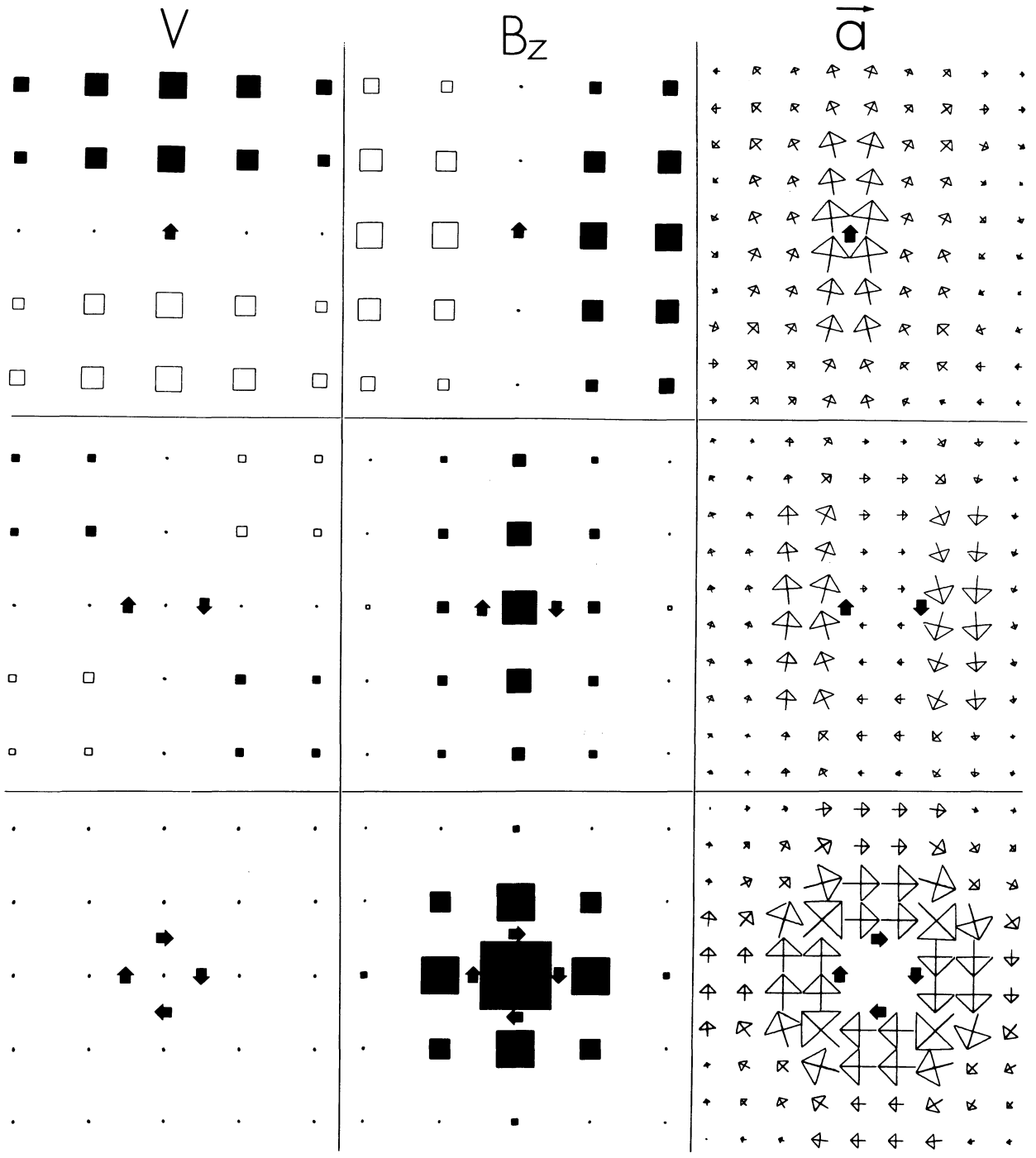

Fig. 7. Two different comparisons are made here: the surface potential (V) vs. the field component normal to the surface (B_z), and the square map of B_z vs. the arrow map of B_z. The side of each square is proportional to V or B_z at that location. The scales are arbitrary but identical down a column. V and B_z and its derivatives were computed in a plane 10 cm above and parallel to the dipoles; squares are separated by 5 cm, arrows by 2.5 cm. The comparison between V and B_z shows the 90° difference for one dipole, and the suppressed potential for two and four dipoles. The comparison between the square and arrow maps of B_z shows that the arrow map is better for visually revealing the dipole combinations used here.

form of display in which arrows are used. The same information is contained in this arrow map as in the square map of Bz. However, by using the arrow map some special information can readily be obtained by visual inspection; this information is the presence of the special dipole combinations. The arrow map is based on $B_{zv}=0$, and if B_{zv} is large, then the arrow map is not valid here. We define each arrow to be the vector

$$\vec{a} = (\partial B_z/\partial y)\hat{x} - (\partial B_z/\partial x)\hat{y} \qquad (7)$$

where $\hat{x}$ and $\hat{y}$ are unit vectors. This is a form of two-dimensional gradient of the scalar quantity Bz and is rotated by 90° from the conventional gradient. When the source is a single dipole the arrows are largest and colinear with the dipole, just over the dipole. This is shown in the arrow map of one dipole, in Fig. 7. One purpose of Fig. 7 is to compare the arrow map with the square map of Bz due to one, two, and four dipoles. Bz and derivatives were computed from eqn. (4). We see that the arrow map reveals the location of the dipoles more effectively to the eye than does the square maps of Bz, especially for two or more dipoles, our cases of interest.

Any scalar field, magnetic or otherwise, can be displayed in this way if desired. This arrow display has the same information content as other displays of the same field, and is only an aid to the eye. Again, it reveals those dipole combinations which we particularly seek with magnetic measurements. It should be noted that the same type of arrow map is not useful for the display of the heart's potential, that is, as a substitute for the isopotential map. This is because those dipole arrangements which give full, unsuppressed potentials (but suppressed Bz) do not stand out in this display. The basic combination here is the in-line opposing dipole pair. The in-line and side-by-side dipole pairs are complementary, and are explained by the 90° rotation between magnetic and electric fields. The former is best measured by the surface potentials, the latter by the external magnetic field. Both potential and magnetic measurements therefore are needed for a full determination of dipoles of the heart.

REFERENCES

1. COHEN, D AND MCCAUGHAN, D: Magnetocardiograms and their variation over the chest in normal subjects. Am J Cardiol 29:678, 1972
2. COHEN, D, HOSAKA, H, LEPESCHKIN, E, MASSELL, B F AND MYERS, G: Abnormal patterns and physiological variations in magnetocardiograms; the first paper in this group of four
3. PLONSEY, R: Capability and limitations of electrocardiography and magnetcardiography. IEEE Trans Bio-Med Eng BME-19#3:239, 1972
4. COHEN, D: Magnetic fields of the human body. Physics Today 28#8:34, Aug 1975
5. HORACEK, B M: Digital model for studies in magnetocardiography. IEEE Trans Mag MAG-9#3:440, 1973
6. CUFFIN, B N: Model Studies of Electrocardiograms and Magnetocardiograms Using Realistic Torso Boundaries. PhD Thesis, Dept of Electrical Engineering, the Pennsylvania State University, University Park, PA. Supervisor: D B Geselowitz, 1974
7. MILLER, W T, III AND GESELOWITZ, D B: Use of electric and magnetic data to obtain a multiple dipole inverse cardiac generator: A spherical study. Ann Biomed Eng 2:343, 1974
8. BAULE, G M: Magnetic Detection of the Heart's Electrical Activity. PhD Thesis, Dept of Electrical Engineering, Syracuse University, Syracuse, N.Y. Supervisor: R McFee, 1964
9. BAULE, G AND MCFEE, R: Theory of magnetic detection of the heart's electrical activity. J Appl Phys 36#6:2066, 1965
10. In a private communication to the author from Professor K SYMON, who had discussed this property with his colleagues of the Physics Department at the University of Wisconsin, including Professor KERST
11. GESELOWITZ, D: On the magnetic field generated outside an inhomogeneous volume conductor by internal current sources. IEEE Trans Mag MAG-6#2:346, 1970
12. Second-derivative maps and a variety of other data are presented in the full four-part report, which is available on request from D COHEN, or from National Technical Information Service, #MIT/FBNML-76-1
13. COHEN, D: Measurements of the magnetic fields produced by the human heart, brain, and lungs, IEEE Trans Mag MAG-11#2:694, 1975